LA-UR- 07-1113

Approved for public release; distribution is unlimited.

Title: New insights in to the single-mode Rayleigh Taylor instability

Author(s): P. Ramaprabhu, CCS-2
Guy Dimonte
Y-N Young
A. c. Calder
B. Fryxell

Intended for: Proceedings of the 10th International Workshop on the Physics of Compressible Turbulent Mixing
Paris, July 2006

Los Alamos
NATIONAL LABORATORY
EST. 1943

e-mail: praveen@lanl.gov

New insights in to the single-mode Rayleigh Taylor instability

P. RAMAPRABHU[1], Guy DIMONTE[1], Y-N. YOUNG[2], A.C. CALDER[3] and B. FRYXELL[1]

[1]*Los Alamos National Laboratory, Los Alamos, NM 87545 USA*
[2]*New Jersey Institute of Technology, Newark, NJ 07102, USA*
[3]*University of Chicago, Chicago, IL 60637, USA*

Abstract: The dependence of the single-mode Rayleigh-Taylor (RT) instability on density difference effects is investigated using four different numerical codes. As the density difference driving the flow approaches infinity, bubbles reach a constant terminal velocity, in agreement with the classical result of Layzer [1]. At the same time, spikes are narrow and in free-fall, a result which can be understood through simple drag-buoyancy arguments. The extension of these ideas to finite density differences is characterized by terminal velocity for bubbles early in time in agreement with a corresponding potential flow theory (Goncharov [2]), and an accelerating flow at late-times. The late-time acceleration is a new result and appears to be driven by the formation of Kelvin-Helmholtz rollups, an effect that is not included in existing nonlinear models of RT.

1 INTRODUCTION

A sharp interface separating two fluids of different densities is Rayleigh-Taylor unstable if an acceleration is directed from the light fluid to the heavy. In this paper, we consider only monochromatic or single-mode interfacial perturbations of wavelength λ and amplitude h_0. It has been shown [3] that an understanding of this simple flow is necessary before considering the fully turbulent RT instability. The growth of such perturbations at the interface is at first exponential [4]

$$h = h_0 e^{\gamma t}, \tag{1.1}$$

with a growth rate γ, and then linear in time, with a corresponding terminal velocity given by

$$v = Fr\sqrt{\frac{Ag\lambda}{1+A}}, \tag{1.2}$$

where Fr is a Froude number. The initial growth stage is often referred to as "linear" since only linear terms in the perturbation equations are important, while the latter stage is termed nonlinear. In the nonlinear stage, the light fluid rises as bubbles due to buoyancy, displacing the heavy fluid, which descends as spikes. While (1.1) is an exact result in the absence of viscosity or other stabilizing effects, the behavior of bubbles and spikes in the nonlinear stage as a function of the Atwood number ($A = \frac{\rho_2 - \rho_1}{\rho_2 + \rho_1}$) is controversial due to disagreement among proposed models [2,5,6]. The differences stem from the choice of potential functions and boundary conditions. In this work, we evaluate competing nonlinear models using numerical simulations, and extend their description to late-times. The results are of interest in describing the turbulent growth rate α which can be related to the Froude number of the dominant bubbles in a bubblefront using

$$\alpha = \frac{Fr^2}{8}\frac{\rho_1 + \rho_2}{\rho_2}\frac{D_b}{h_b}. \tag{1.3}$$

Image analysis from the Linear Electric Motor experiments show that $h_b/D_b > 1$ for leading RT bubbles in a turbulent flow. To evaluate bubble dynamics in a regime relevant to turbulent flow, we calculate RT single-mode flow in an elongated box, and at late-times.

2 RESULTS

We report on numerical simulations of the single-mode Rayleigh-Taylor problem up to intermediate and late-times. The calculations were performed using four different codes, and in an elongated box ($\lambda x \lambda x 8\lambda$) to accommodate the late-time growth. 3D perturbations of the form

$$h(x,y) = h_0\{\cos(kx) + \cos(ky)\} \qquad (2.1)$$

were used, with the amplitude chosen such that $kh_0 << 1$. Three of the codes belong to the MILES category, while a fourth Direct Numerical Simulation (DNS) was also employed. Other details of the calculations, including descriptions of the algorithms used are provided in [7].

Figure 2.1 is a plot of the Froude numbers deduced from the intermediate-time saturation velocities of bubbles from the codes used in this study as a function of the Atwood number. All the codes give a constant $Fr = 0.56$ in agreement with [2], but not with [5] and [6] who predict a different functional form for the Froude numbers. This is because the form of potential functions used in [2] satisfies the condition of zero net mass-flux across the interface.

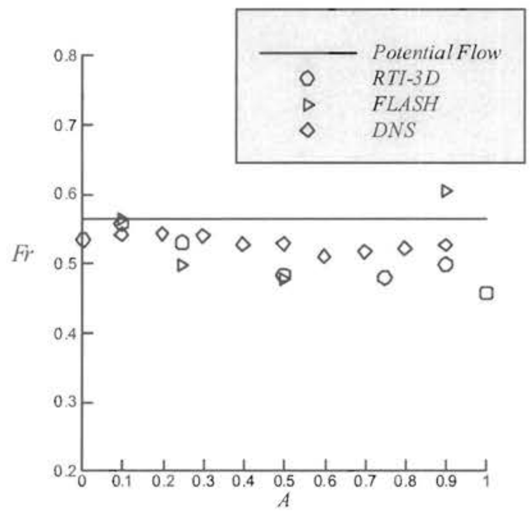

Figure 2.1 Froude numbers from 3D NS and potential flow theory of [2].

While bubbles reach a terminal velocity for intermediate times at all A, figure 2.2 (a) shows that spikes resemble bubble behavior at small A, but accelerate at larger density differences. As $A \rightarrow 1$, $v_s \sim \sqrt{\frac{2A}{1-A}\frac{g}{k}}$ from drag-buoyancy models [8] and potential flow theory of [2] becomes unbounded, and spikes are in free-fall. This can be understood from a simple balance of drag and buoyancy terms on the spike objects:

$$\ddot{h}_s = Ag - C\dot{h}_s^2 \frac{\rho_1}{\rho_1 + \rho_2}\frac{1}{h_s} \qquad (2.2)$$

For $A \rightarrow 1$ ($\rho_1 \rightarrow 0$), equation (2.2) and our NS (figure 2.2 (b)) give $h_s \sim \frac{1}{2}gt^2$. Finally, by applying mass conservation on any horizontal plane, it also follows that as $A \rightarrow 1$, bubble diameters increase while spike diameters become vanishingly small.

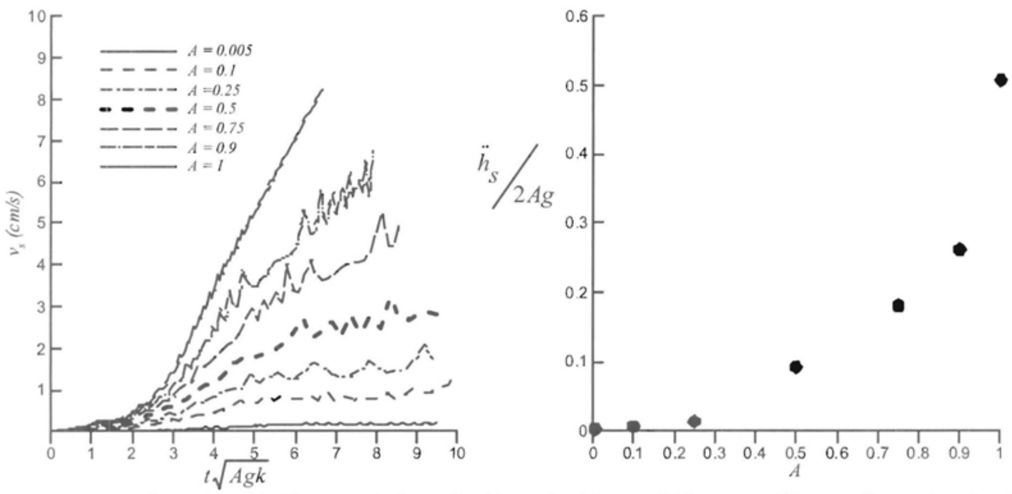

Figure 2.2 (a) Time evolution of spike velocities at different A. (b)Non-dimensional spike acceleration coefficient vs. A.

Figure 2.3 shows the evolution of bubble Froude numbers up to late times for different Atwood numbers. The Froude number is plotted against the bubble aspect ratio h_b/D_b. The small A calculations exhibit a curious acceleration away from the terminal velocity, followed by a saturation to a higher Fr late in time, while the large A cases (A>0.5) remain terminal. This behavior is observed in all of the codes used here, and occurs at $h_b/D_b \sim 1$. Such a deviation from the classical potential flow result has been observed earlier by [9] who attribute the effect to bubble-tip curvature effects. However, our image analysis indicates that this is not the case.

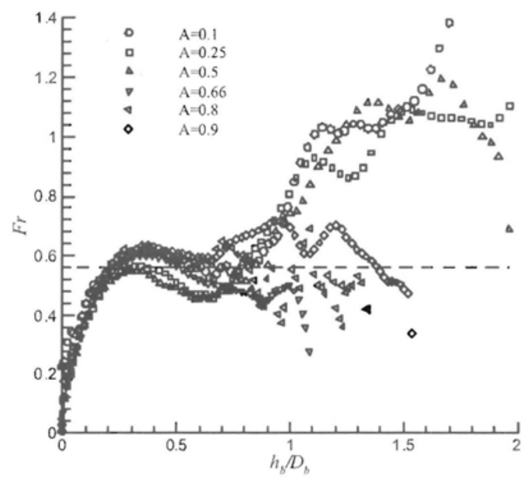

Figure 2.3 Time history of bubble Froude numbers from NS at different A.

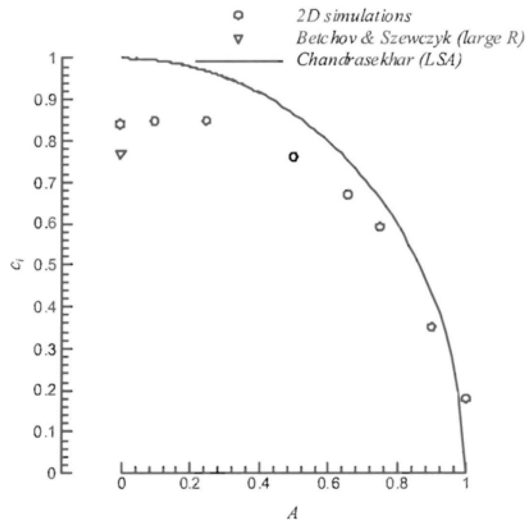

Figure 2.4 Kelvin-Helmholtz growth rates from 2D NS and linear stability theory.

We attribute the observed behavior to the formation of secondary Kelvin-Helmholtz (KH) vortices on the neck of the bubbles at small density differences. The induced flow from such secondary vortices creates a momentum jet that accelerates the bubbles to a higher Froude number. Such a mechanism has been identified in boosting the rise velocity of turbulent RT bubbles [10], and by certain species of fish to propel themselves [11]. However, note that the appearance of secondary KH instabilities in RT is confined to small density differences. This is consistent with linear stability analysis of KH flow [4] which suggests that at large density differences, the shear layer growth c_i is suppressed inertially according to

$$c_i = \pm\sqrt{-k_x^2(\Delta U)^2 \frac{\rho_1\rho_2}{(\rho_1+\rho_2)^2}}, \tag{2.3}$$

where ΔU is the velocity difference driving the flow. Thus, from (2.3) $c_i \rightarrow 0$ for A $\rightarrow$ 1. This is also observed in our 2D simulations of KH flow, the growth rates from which are summarized in figure 2.4. The calculations used a square domain (λxλ) with the velocity contrast ΔU spread across 3 zones and g = 0, since buoyancy is not relevant here. Our calculations which correspond to a piecewise linear profile are in good agreement with the linear stability analysis of [4] who assumed a step-function for the velocity profile, and with [12] who considered a tangent hyperbolic function. Furthermore, the growth rates from theory and NS are only weakly sensitive to A for small density differences. This explains why the observed acceleration in RT appears at approximately the same point in time for cases with small A (at $h_b/D_b \sim 1$), since the growth rates of the underlying KH instability remains nearly uniform under such conditions.

These ideas can be further verified by quantifying the size of secondary vortex cores in RT for different A. We adopt the definition proposed by [13] that identifies connected regions with two negative eigen-values of the velocity gradient tensor as a vortex. This condition ensures that a local pressure minimum exists in a vortex core, while at the same time eliminating false positives due to unsteady straining and viscous effects. Figure 2.5 shows the evolution of the % volume occupied by vortex cores (identified using this technique) within the computational domain, as a function of h_b/D_b at A = 0.005 and 1.0. Clearly, there is a sudden development of secondary vortex structures near $h_b/D_b \sim 1$, for the low Atwood case. This event coincides with the onset of the observed acceleration. Conversely, the high Atwood case shows no such trend, consistent with the lack of observed acceleration.

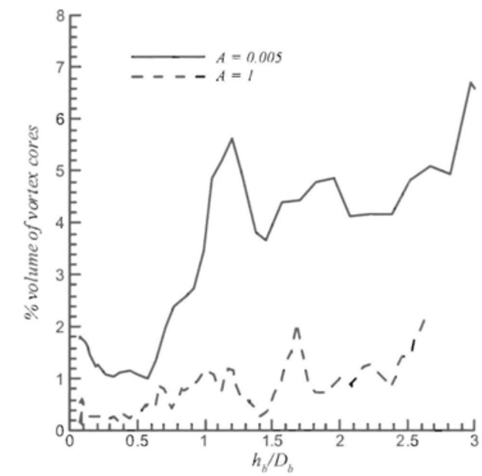

Figure 2.5 Evolution of % volume of computational box occupied by vortex cores at A = .005 and 1.0.

3 SUMMARY

We have investigated the single-mode Rayleigh -Taylor instability in a long box, and at late-times, so that the results bear direct relevance to the turbulent flow. We find that initially, the nonlinear flow is in agreement with the model of [2], because their choice of the velocity potential function satisfies the no flux condition across the interface. At late-times, the behavior depends on the Atwood number. At small A, secondary Kelvin-Helmholtz vortices form on the neck of the primary bubble, the induced flow from which accelerates the bubbles away from the expected terminal velocity. The formation of KH vortices at large A is suppressed, consistent with the linear stability theory of [4]. We conclude that potential flow models are accurate in the regime they are applicable (at high A). At low A, the development of secondary instabilities complicate the evolution due to the associated vertical momentum jet propelling the bubbles forward. We suggest further numerical simulations of this simple problem to verify our conclusions.

REFERENCES

[1] D. Layzer, Astrophys. J 122, 1 (1955).
[2] V.N. Goncharov, Phys. Rev. Lett. **88**, 134502 (2002).
[3] Guy Dimonte, Phys. Rev. E **69**, 056305 (2004).
[4] S. Chandrasekhar, *Hydrodynamic and Hydromagnetic Stability* (Oxford University Press, Oxford, 1961).
[5] S-I. Sohn, Phys. Rev. E 67, 26301 (2003).
[6] S. I. Abarzhi, K. Nishihara, and J. Glimm, Phys. Letters A 317, 470 (2003).
[7] P. Ramaprabhu, Guy Dimonte, Y_N. Young, A.C. Calder, B. Fryxell, Phys. Rev. E 74, 066308 (2006).
[8] D. Oron et al., Phys. Plasmas **8**, 2883 (2001).
[9] J. Glimm *et al.*, Phys. Fluids **A 2**, 2046 (1990).
[10] N.A. Inagamov *et al.*, J. Expt. Theo. Phys. **92(4)**, 715 (2001).
[11] F.E. Fish & G.V. Lauder, Ann. Rev. Fluid Mech. **38**, 192 (2006)
[12] R. Betchov and A. Szewczyk, Phys. Fluids **6**, 1391 (1963).
[13] J. Jeong and F. Hussain, J. Fluid Mech. **285**, 69 (1995).